JCTC Journal of Chemical Theory and Computation

Article

pubs.acs.org/JCTC

Structure−Properties Relationships in Triplet Ground State Organic Diradicals: A Computational Study

Vincenzo Barone,[†] Corentin Boilleau,[†] Ivo Cacelli,[‡] Alessandro Ferretti,[§] Susanna Monti,[†,§] and Giacomo Prampolini*[,∥]

[†]Scuola Normale Superiore, piazza dei Cavalieri 7, I-56126 Pisa, Italy

[‡]Dipartimento di Chimica e Chimica Industriale, Università degli Studi di Pisa, via Risorgimento 35, I-56126 Pisa, Italy

[§]Istituto di Chimica dei Composti OrganoMetallici (ICCOM-CNR), Area della Ricerca, via G. Moruzzi 1, I-56124 Pisa, Italy

[∥]Istituto per i Processi Chimico-Fisici (IPCF-CNR), Area della Ricerca, via G. Moruzzi 1, I-56124 Pisa, Italy

ABSTRACT: A fast and efficient computational protocol, devised for the accurate calculation of singlet−triplet magnetic splittings in organic diradicals, is here applied to several promising organic magnets, recently considered in the literature. The very good agreement with the measured values, obtained for all investigated compounds, suggests that the present approach could successfully flank the experiment in the design of novel magnetic materials. Indeed, some structure−magnetic properties relationships were rationalized thanks to the theoretical soundness of the adopted multireference approach. In particular the different effects of N· and NO· magnetic moieties, as well as the role of lateral aliphatic chains and phenyl pendant substituents, are discussed in detail.

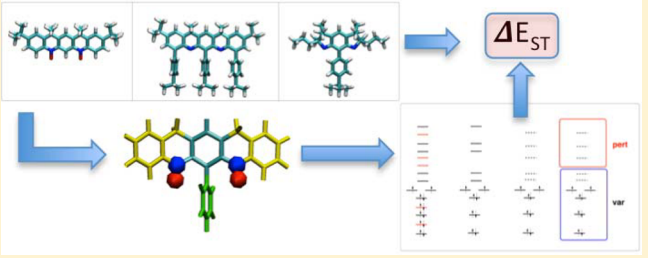

1. INTRODUCTION

Organic magnetic materials[1−8] have attracted a large and growing amount of interest due to their potential use in magnetic resonance imaging, as contrast agents or spin labels,[9−11] in controlled radical polymerization,[12] and in many devices in the field of spintronics (e.g., sensing, memory, or switching devices).[1,2,13−18] In their design, an important role[2,6,19−24] can be played by ladder high spin poly radicals,[25−28] which can be obtained by assembling specific diradicals.[8,29−31] To be successfully employed in the preparation of efficient organic magnets, these diradicals need to satisfy two main conditions: they should be stable at room temperature and possess a large singlet−triplet energy gap (ΔE_{ST}). As far as the first issue is concerned, despite most of the organic molecules with triplet ground states being typically short-lived, recent findings by Rajca and co-workers[8,24,32,33] have shown that "magnetic functional groups" like N· or NO· may gain significant protection (hence increased stability) when linked to an *m*-phenylene unit embedded in a rigid polycyclic structure. On the other hand, specific substituents can strongly tune ΔE_{ST}.[24,32−34] Unfortunately, this energy gap is not directly accessible by experiments, but it can only be derived through a numerical fit[12,17,32,35−40] from the temperature dependence of the magnetic susceptibility. For ferromagnetic interactions, the sensitivity of this method to the values of ΔE_{ST} in solution is rather small[1,32,40,41] and often allows only for a determination of a lower limit of ΔE_{ST}.[32,40] In this framework, it may be rather difficult to rationalize the effect of different substituents on ΔE_{ST} only on the basis of experimental data.

A crucial aid to understanding structure−magnetic property relationships can be offered by theoretical approaches, provided an accurate yet feasible computational protocol is devised. In fact, the calculation of ΔE_{ST} (i.e., $E_S - E_T$) is still challenging, as diradicals of interest are rather large molecules, mostly made by magnetic moieties bridged by aromatic or other unsaturated fragments, which modulate the coupling between the unpaired spins. Although computational convenience would suggest resorting to Density Functional Theory (DFT), adopting the Noodleman broken-symmetry (BS) method[42,43] to calculate the magnetic splitting, this level of theory tends to overestimate the value of ΔE_{ST} for triplet ground state molecules.[33,44,45] Moreover, both theoretical foundation and robustness are not without problems, and care should be taken in relying on BS-DFT results to interpret the subtle effects governing the ferro- and anti-ferromagneticity. As far as post-HF methods are concerned, the neglect of interaction terms between the perturbers that characterizes methods based on second order perturbation theory significantly reduces the accuracy of the results,[46] whereas multireference variational approaches[47−56] appear to be much more reliable.

In this framework, the Dedicated Difference Configuration Interaction (DDCI) scheme[48,57,58] is particularly appealing due to its definition of the variational space in well-defined *a priori* terms (see Table 1) without resorting to arbitrary choices. Unfortunately, reduced versions of the approach (the so-called

Received: September 11, 2012
Published: November 16, 2012

   dx.doi.org/10.1021/ct300790c | *J. Chem. Theory Comput.* 2013, 9, 300−307

Table 1. Configurational Classes Considered within the DDCI Scheme[a]

class	description	class[58]
N.2.0	the primary four dimensional space (includes kinetic exchange)	
N.1.1	single excitations from magnetic orbitals	1p
N.0.2	double excitations from magnetic orbitals	2p
N-1.3.0	single excitations from core to magnetic orbitals (related to superexchange)	1h
N-1.2.1	single excitations to core to unoccupied orbitals (include spin polarization)	1h+1p
N-2.4.2	double excitations from core to magnetic orbitals	2h
N-1.1.2	simultaneous excitations from core and magnetic to unoccupied orbitals	1h + 2p
N-2.3.1	double excitations from core to magnetic and unoccupied orbitals	2h + 2p

[a]Note that within the DDCI2 scheme the classes reported in the last two rows are not considered. Each class is labeled in terms of three numbers (first column) referring to core, magnetic, and unoccupied molecular orbitals, respectively. In the last column the corresponding notation proposed by Calzado et al.[58] is reported.

DDCI2 model) are not always satisfactory, and the complete DDCI space becomes unmanageable for large systems. In order to extend the range of applicability of the DDCI scheme, without a significant loss of accuracy, a new integrated strategy for an accurate calculation of singlet−triplet magnetic splittings has been recently proposed by our group[34,59−61] and schematized in Figure 1. The computational protocol

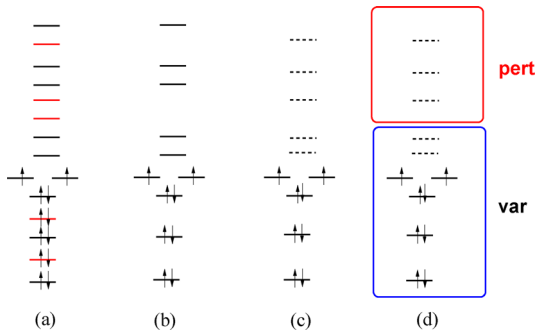

Figure 1. Scheme of the three-step strategy. (a) Molecular orbitals are localized into primary (black) and secondary (red) fragments. (b) Step I: MOs on secondary fragments are excluded from DDCI calculations. (c) Step II: MVOs (on the primary fragment) are determined as eigenvectors of a modified Fock operator (dashed lines). (d) Step III: Only variationally active virtual orbitals are considered together with the occupied MOs (blue window) for a variational treatment, whereas the rest of the MVOs (red window) are taken into account through a perturbative approach.

essentially consists of three steps to be undertaken within the DDCI scheme. First, the DDCI configurational space is reduced by fragmentation/localization criteria.[59] Thereafter, the CI convergence is accelerated employing a set of suitably Modified Virtual Orbitals (MVO).[60] Finally, the application of the Complementary Space Perturbative Approach (CSPA)[61] allows for a further reduction of the dimensions of the variationally treated space without a sensible loss of accuracy. This strategy, which permits treating large molecules at a reasonable computational cost, was successfully validated on several organic diradicals,[34,62,63] yielding ΔE_{ST} values in good agreement with the experimental estimates.

In this paper, we apply our protocol to different classes of ferromagnetic organic diradicals recently synthesized by the group of Rajca[24,32,33] (see Figure 2), all characterized by a remarkable stability at room temperature. Although all of these compounds, namely diarylnitroxide,[32] aminyl,[33] and aza-*m*-xylylene[24] diradicals, have the same *m*-phenylene central unit, their magnetic properties are rather different, and experimental estimates of the singlet−triplet energy gap vary by 1 order of magnitude, going from $\Delta E_{ST} \geq 0.6$ kcal/mol[32] to ≥2 kcal/mol[33] up to ∼10 kcal/mol.[24]

The aim of our work is to clarify how the different structural motifs, in which the parent *m*-phenylene unit is embedded, affect the spin−spin coupling between the magnetic moieties. Indeed, a deeper understanding of such a mechanism could help in designing novel materials, with obvious benefits in terms of costs and time. In a previous work,[63] we applied the three-step DDCI approach to the diarylnitroxide diradical, obtaining quantitative agreement with the experimental value of ΔE_{ST} = 0.6 kcal/mol, in contrast with DFT-BS calculations[32] that overestimated the singlet−triplet gap of 2 kcal/mol. In this work, we apply our computational protocol to both the aminyl and aza-*m*-xylylene diradicals and compare the results with both experimental measures and literature DFT calculations. Finally, for comparison purposes, we consider a nitroxy homologue of the aza-*m*-xylylene, which, to the best of our knowledge, has not yet been synthesized.

The paper is organized as follows: In the next section, computational details are given, whereas results are discussed in section 3. Main conclusions will be drawn in the last section.

2. METHODS AND COMPUTATIONAL DETAILS

The molecular geometry of the triplet state of all systems was optimized at the DFT-UB3LYP/cc-pvdz level of theory using the Gaussian 09 package.[64] At the equilibrium geometry, the canonical molecular orbitals (MOs) to be used in the post-HF calculations were obtained by a ROHF calculation for the triplet state, using the Gamess code,[65] with the 6-31G(d) basis set.

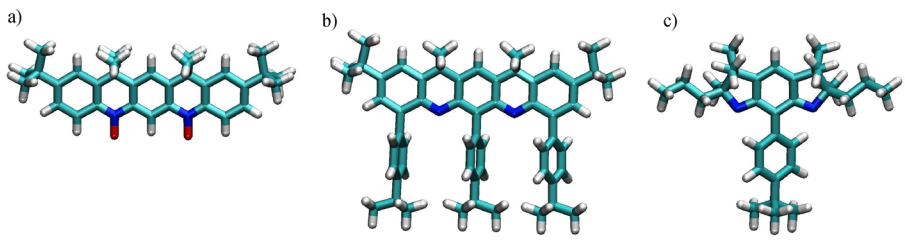

Figure 2. Organic diradicals recently synthesized and studied by Rajca and co-workers. (a) Diarylnitroxide,[32] (b) aminyl,[33] and (c) aza-*m*-xylylene.[24] Atom colors are cyan, white, blue, and red for C, H, N, and O, respectively.

dx.doi.org/10.1021/ct300790c | J. Chem. Theory Comput. 2013, 9, 300−307

The three-step protocol was then applied as follows:

Step I: Fragmentation and Localization. MOs are first localized onto specific moieties through the Pipek–Mezey method.[66] Only those MOs belonging to the fragment more involved in the magnetic interaction are retained for the DDCI calculation,[59,67] whose configurational classes are reported in Table 1. This fragment is therefore named "primary," whereas the remaining ones are referred to as "secondary."

Step II: Modified Virtual Orbitals (MVO). MVOs are determined by the following eigenvalue equation projected on the virtual orbital space

$$(\hat{F} + \hat{V})\phi_\mu = \varepsilon_\mu \phi_\mu \tag{1}$$

where $\hat{F}$ is the Fock operator for the restricted triplet state and $\hat{V}$ is a supplementary nuclear potential obtained placing some extra charges on the atoms bearing the magnetic orbitals. The effective optimal supplementary charges were set to $2e$, as determined in previous work.[61]

Step III: CI + CSPA. In the hypothesis that only the interaction terms between the lowest energy configurations affect ΔE_{ST}, the virtual orbitals space is partitioned in active (lowest energy MVOs) and inactive subspaces, with reference to the variational calculation. The configurations involving the first set are included in the CI treatment, whereas those involving inactive MVOs are included in the perturbative treatment, according to the Complementary Space Perturbative Approach (CSPA) using the so-called barycentric Möller–Plesset partition. The virtual MOs belonging to the first space are called Variationally Active Virtual Orbitals (VAVO).

The whole procedure is reported in a pictorial representation in Figure 1, and more details can be found in the original papers.[34,59−61]

The MVOs were obtained using the Fortran program QUIOLA coded by the authors, which interfaces the GAMESS output files with the routine for the transformation of the integrals from the atomic to the molecular basis set.[67] Both CI and CSPA were implemented in the BALOO program, which has been coded in our group and will be presented elsewhere. In all calculations, all 1s core orbitals were always kept inactive with occupation number 2 in all configurations, both in the variational and perturbative calculations.

In order to better rationalize the computational results, it may be useful to recall the minimal description of magnetic interactions in a diradical system, which can be given within a CAS(2,2) four-dimensional configurational space. Within the valence bond framework, this can be easily obtained considering the two localized magnetic orbitals $|\phi_a\rangle$ and $|\phi_b\rangle$ to generate the four basic configurations:

$$|^1\Psi_A\rangle = \frac{1}{\sqrt{2}}(|...\phi_a\bar{\phi}_b\rangle + |...\phi_b\bar{\phi}_a\rangle)$$
$$|^1\Psi_B\rangle = |...\phi_a\bar{\phi}_a\rangle$$
$$|^1\Psi_C\rangle = |...\phi_b\bar{\phi}_b\rangle$$
$$|^3\Psi\rangle = \frac{1}{\sqrt{2}}(|...\phi_a\bar{\phi}_b\rangle - |...\phi_b\bar{\phi}_a\rangle) \tag{2}$$

Among the resulting states, $|^1\Psi_A\rangle$ and $|^3\Psi\rangle$ provide the main contribution to the singlet–triplet energy gap, since the charge transfer (CT) configurations ($|^1\Psi_B\rangle$ and $|^1\Psi_C\rangle$) lie at higher energies. Despite this minimal configurational space alone being insufficient to provide a reliable estimate of the ΔE_{ST} ($E_S - E_T$) gap, it can be useful for interpretative aims, since, based on a perturbation approach, the gap can be easily expressed[47,58] as

$$\Delta E_{ST} = 2K_{ab} - \frac{4t_{ab}^2}{U} \tag{3}$$

where K_{ab} is the direct exchange integral between the two localized orbitals, t_{ab} is the hopping term ($\langle\phi_a\bar{\phi}_a|\phi_a\bar{\phi}_b\rangle = \langle\phi_b\bar{\phi}_b|\phi_a\bar{\phi}_b\rangle$) between the two magnetic centers, and U is the relative energy of the CT configurations with respect to the neutral ones. It may be worth noticing that the exchange term is the ferromagnetic part of the gap, whereas the last term of eq 3 is the antiferromagnetic part.

3. RESULTS

3.1. Diarylnitroxide and Aminyl Diradicals. The organic diradicals recently synthesized by Rajca and co-workers[24,32,33] and the object of this study are reported in Figure 2.

As far as the diarylnitroxide and aminyl diradical (first two panels of Figure 2) are concerned, to further reduce the computational burden, calculations were performed on slightly smaller homologues, derived from the parent diradicals by dropping some substituents (as external *tert*-butyl or phenyl groups) located far from the central *m*-phenylene core bearing the magnetic units. Clearly, all substituents relevant for the modulation of ΔE_{ST} were maintained. These molecules, displayed in Figure 3, are composed of three aromatic rings

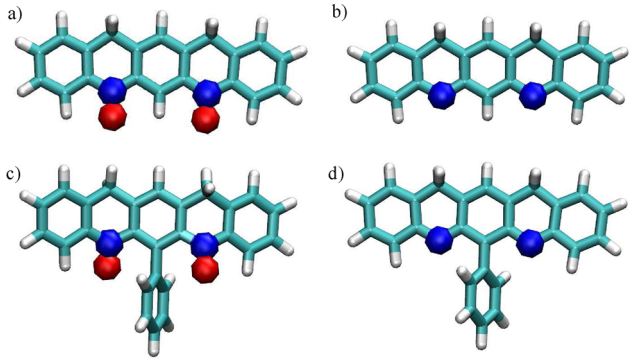

Figure 3. First set of target organic diradicals. (a) Diarylnitroxide diradical $\mathbf{D}_1$; (b) aminyl diradical $\mathbf{D}_2$; (c) diarylnitroxide diradical with pendant phenyl $\mathbf{Dp}_1$; (d) aminyl diradical with pendant phenyl $\mathbf{Dp}_2$. Atoms bearing the magnetic orbitals are evidenced with blue (N) and red (O) spheres.

interspersed by six-membered aliphatic rings containing the magnetic groups NO· (left top panel, diarylnitroxide diradical $\mathbf{D}_1$) or N· (right top panel, amynil diradical $\mathbf{D}_2$). A pendant aromatic ring is added in the $\mathbf{Dp}_1$ and $\mathbf{Dp}_2$ systems (left and right bottom panels, respectively). Among these, the $\mathbf{D}_1$ and $\mathbf{Dp}_2$ molecules are strictly related to the experimentally studied molecules displayed in Figure 2. Conversely, diradicals $\mathbf{Dp}_1$ and $\mathbf{D}_2$, which to the best of our knowledge have not been yet synthesized, are considered in order to obtain a sound and complete rationalization of how the different substitutions influence the magnetic splitting. In fact, these four species are characterized by the presence/absence of oxygen at the magnetic sites and by the presence/absence of a pendant ring linked to the central aromatic ring half way between the magnetic sites. A cross comparison between these four systems will help to generate an understanding of how the singlet–

triplet energy gap is affected by the different magnetic groups and/or by the presence of the pendant ring. Despite calculations on diradical $\mathbf{D}_1$ having already been reported in a previous work,[63] they have been repeated for validation purposes with the new BALOO code, obtaining results in quantitative agreement with those already published, which were obtained using a modified version of the Cipsi[61] code.

For all four diradicals, several fragmentation routes were followed both for interpretative purposes and to gain experience in devising criteria to identify the importance of different moieties in modulating the magnetic coupling. The different fragmentation strategies are shown in Figure 4 for the $\mathbf{Dp}_1$ diradical, and the same routes were followed for all of the other systems. In the first fragmentation scheme (route **1**), only the group bearing the magnetic orbitals (i.e., N or NO) and those of the phenyl bridge in between were assigned to the primary fragment, whereas in route **2** the primary fragment was augmented by adding all atoms of the polycyclic structure, leaving only the phenyl pendant (when present) in the secondary fragment. This latter route was further divided into two different schemes, in which only the π (route **2a**) or all (**2b**) orbitals localized on the external fragments (see Figure 4) were considered in the DDCI space.

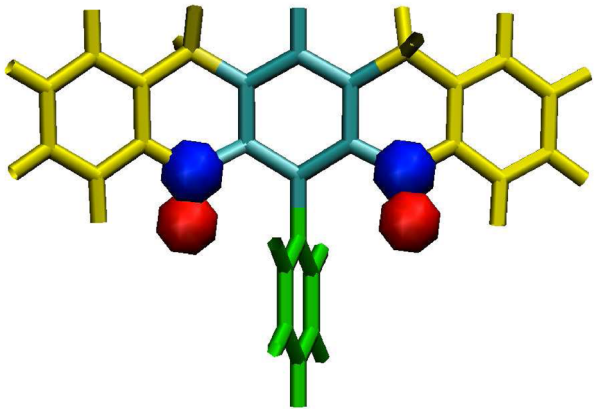

Figure 4. Fragmentation routes applied to diradical $\mathbf{Dp}_1$. Cyan: primary fragment in route **1**. Yellow: fragment added to the primary fragment in route **2**. Green: secondary fragment in all calculations. Atoms bearing the magnetic orbitals are always in the primary fragment and are evidenced with blue (N) and red (O) spheres. The same schemes have been applied to all homologues $\mathbf{D}_1$, $\mathbf{D}_2$, and $\mathbf{Dp}_2$.

In previous works,[34,63] we were able to propose and validate the rule of thumb that a reliable ΔE_{ST} value can be obtained in the CSPA scheme by using a VAVO/VO (i.e., the ratio between variationally active virtual orbitals and all considered VOs) of at least 30%. In this work, we want to control again the convergence of VAVO/VO by comparing, for the smaller active fragments (route **1**), the results obtained with values in the 40−80% range with those computed by variationally handling the full DDCI space (VAVO/VO = 100%). By looking at Table 2, it is apparent that the proposed approach allows for a considerable reduction of the variational space, without a significant loss of accuracy. Indeed, in all cases, thanks to the combination of the MVO approach with the CSPA, a converged value of ΔE_{ST} is reached by treating variationally only the 40−60% of the VOs, with obvious savings in computational time and feasibility. In fact, the difference between the full variational reference value and the ones obtained by applying the CSPA is negligible down to a 60% VAVO/VO ratio and amounts to a few cm^{-1} for a 40% ratio. For these reasons, considering the large molecular dimensions of diradicals with pendant phenyl, calculations for $\mathbf{Dp}_1$ and $\mathbf{Dp}_2$ were performed only up to a VAVO/VO ratio of 50% when using the expensive fragmentation route **2b** (almost 7 million Slater determinants).

Table 2. DDCI Results for Target Diradicals $\mathbf{D}_1$ and $\mathbf{Dp}_1$[a]

$\mathbf{D}_1$					
fragm. route	VAVO/VO (%)	Vdim (10^3)	ΔE_{ST}^V (cm^{-1})	ΔE_{ST} (cm^{-1})	ΔE_{ST} (kcal/mol)
1	40	632	239	200	0.57
1	60	1090	215	215	0.62
1	80	1670	216	216	0.62
1	100	2370	218	218	0.62
2b	20	1393	225	165	0.47
2b	40	2238	215	182	0.52
2b	60	7425	214	183	0.53
$\mathbf{Dp}_1$					
fragm. route	VAVO/VO (%)	Vdim (10^3)	ΔE_{ST}^V (cm^{-1})	ΔE_{ST} (cm^{-1})	ΔE_{ST} (kcal/mol)
1	40	448	232	181	0.52
1	60	846	228	183	0.53
1	80	1365	222	184	0.53
1	100	2563	187	187	0.54
2b	20	1372	204	143	0.41
2b	30	3160	200	148	0.42
2b	40	5586	199	149	0.42

[a]Fragmentation route employed and VAVO/VO ratio are reported in the first two columns. In the third and fourth columns, the dimension (in detors) of the DDCI space treated variationally (Vdim) and the magnetic splitting (ΔE_{ST}^V) obtained by a pure variational calculation in such space are reported. In the last two columns, the CSPA corrected value is reported in cm^{-1} and kcal/mol, respectively.

In agreement with the experimental estimates[32] ($\Delta E_{ST} \sim 0.6$ kcal/mol for molecule *a* in Figure 2), the magnetic splittings of diradicals $\mathbf{D}_1$ and $\mathbf{Dp}_1$ are rather small, amounting to 0.5 and 0.4 kcal/mol, respectively. In both cases, the effect of increasing the DDCI space by considering the secondary fragments results in a slight reduction (~0.1 kcal/mol) of the gap. Similarly, the presence of the phenyl pendant does not introduce significant changes, the computed ΔE_{ST} differing by ~0.1 kcal/mol for the two targets. Turning to the aminyl diradicals, despite the significant differences observed among the various routes (which will be discussed below), we may see that the results reported in Table 3 are again in agreement with experimental values, where a lower bound estimate of 2 kcal/mol for ΔE_{ST} was found[33] for molecule b of Figure 2, while 4.7 and 5.5 kcal/mol are the best values computed for diradicals $\mathbf{D}_2$ and $\mathbf{Dp}_2$, respectively.

The proposed approach is thus able to account for the impressive increase of the magnetic splitting observed experimentally for the aminyl based diradicals, with respect to their diarylnitroxide homologues. Indeed, after the substitution of the −NO· moiety by the −N· one, the ΔE_{ST} of both **D** and **Dp** increases by almost 1 order of magnitude. One possible rationalization of this striking effect is that the presence of the oxygen atoms draws electron density away from the *m*-phenylene ring, reducing its effectiveness as a "magnetic bridge." This hypothesis is supported by a Mulliken population analysis performed on the localized magnetic orbitals ($|\phi_a\rangle$ and $|\phi_b\rangle$), resulting from a mixing of the two canonical magnetic

dx.doi.org/10.1021/ct300790c | J. Chem. Theory Comput. 2013, 9, 300−307

Table 3. DDCI Results for Diradicals D_2 and Dp_2[a]

D_2					
fragm. route	VAVO/VO (%)	Vdim (10^3)	ΔE_{ST}^V (cm^{-1})	ΔE_{ST} (cm^{-1})	ΔE_{ST} (kcal/mol)
1	40	264	3524	3419	9.78
1	60	535	3142	3420	9.78
1	80	899	3422	3423	9.79
1	100	1354	3424	3424	9.79
2a	40	1090	2372	2397	6.84
2a	60	1670	2357	2397	6.84
2a	80	2370	2393	2399	6.84
2b	30	2956	1773	1653	4.73
2b	50	4992	1708	1654	4.73
2b	60	6458	1731	1655	4.73
Dp_2					
fragm. route	VAVO/VO (%)	Vdim (10^3)	ΔE_{ST}^V (cm^{-1})	ΔE_{ST} (cm^{-1})	ΔE_{ST} (kcal/mol)
1	40	257	3753	3693	10.55
1	60	516	3702	3697	10.55
1	100	1157	3698	3698	10.55
2b	30	2596	2062	1915	5.52
2b	40	4992	1991	1915	5.52
2b	50	6622	1976	1918	5.52

[a]Fragmentation route and VAVO/VO ratio are reported in the first two columns. In the third and fourth columns, the dimension of the DDCI space treated variationally (Vdim) and the magnetic splitting (ΔE_{ST}^V) obtained by a pure variational calculation in such a space are reported. In the last two columns, the CSPA corrected value is reported in cm^{-1} and kcal/mol, respectively.

orbitals. The results are reported in Table 4 for one magnetic orbital, the second one showing almost identical Mulliken

Table 4. Mulliken Charges of the Localized Magnetic Orbitals for the Four Magnetic Systems in the High Spin HF-SCF State[a]

diradical	N· or NO·	central ring	lateral rings	other
D_1	0.905	0.047	0.045	0.003
Dp_1	0.921	0.038	0.036	0.005
D_2	0.626	0.192	0.166	0.015
Dp_2	0.606	0.208	0.163	0.022

[a]The charge density of the two localized magnetic orbitals is practically identical.

charges. It appears that the oxygen atoms sensibly diminish the extension of the magnetic orbitals over the rest of the molecule ($\leq$0.1), because of a strong localization over the nitroxide group ($\sim$0.9).

Conversely, in the aminyl diradicals D_2 and Dp_2, a larger fraction ($\geq$0.3) of the magnetic canonical orbitals can be ascribed to atoms other than nitrogen. Each magnetic orbital of D_2 and Dp_2 shows about 0.20*e* on the central ring and 0.16*e* on the lateral rings. The reason of such differences in charge delocalization of the magnetic orbitals deserves some comments. The magnetic orbitals of the NO· and N· groups are different in nature: the first corresponds to the antibonding π_{NO}^*, whereas the second is the atomic lone pair π_N of nitrogen. Therefore, the second one has a unit charge on N, whereas in the first one the charge on N is about one-half, and the interaction with the orbitals of the neighboring carbon atoms is expected to be more effective for π_N rather than for π_{NO}^*. This increased delocalization in aminyl compounds has two main consequences: (i) As discussed in a previous paper,[59] a large delocalization on the central ring has the effect of increasing the exchange integral (K_{ab}, see eq 3) between the localized magnetic orbitals. As minor changes are observed in the hopping term t_{ab}, the contribution of the CT configurations is not increased correspondingly, and the expected result is a strong stabilization of the triplet state. (ii) The delocalization on the lateral rings makes the cheaper fragmentation route **1** rather questionable, since the dynamical correlation included in the DDCI scheme neglects the portion of the magnetic orbitals on the lateral fragments (we remind the reader that in the DDCI scheme only the magnetic orbitals are fully correlated). In particular, the inclusion of the correlation of the magnetic orbitals in the lateral fragments is expected to favor the singlet state for the following reason. According to eq 3, such a state contains small contributions of the CT configurations, in which one electron migrates from one side of the molecule to the opposite one. These, which do not contribute to the triplet state, are very sensitive to polarization/relaxation effects due to the inadequate form of the molecular orbitals,[68] specifically optimized for a wave function which assures neutrality on each molecular moiety. Thus, an increase in delocalization of the magnetic orbitals toward the lateral fragments is expected to stabilize the CT configurations. Therefore, the inclusion of the dynamical correlation in the lateral regions should favor the singlet state, decreasing the energy gap. This effect is expected to be more effective for the N· based systems, which are more strongly delocalized with respect to their NO· homologues.

These considerations agree well with the results of Table 3, even if the ΔE_{ST} change on going from route **1** to route **2** is surprisingly high (from 9.8 to 4.7 kcal/mol for D_2). Notice that this effect of correlation on the lateral rings also affects both D_1 and Dp_1 systems (see Table 2), albeit by a much smaller entity.

As far as the effect of the pendant phenyl is concerned, a much smaller change is observed in ΔE_{ST}, −0.1 and 0.8 kcal/mol for diarylnitroxide (Table 2) and aminyl (Table 3), respectively. The changes are of different signs in the two classes of molecules: in the NO based molecules, the pendant phenyl stabilizes the singlet state, and the opposite is found for the N based molecules. These results are fully consistent with the observed charge delocalization in the central ring, shown in the population analysis reported in Table 4. In fact, for the NO based molecules, the pendant phenyl group tends to decrease the charge on the central ring with a corresponding decrease of the energy gap. The opposite is found for the N based molecules: the triplet is stabilized by the pendant phenyl. It may be worth stating again that the central ring acts as a ferromagnetic bridge for *meta* substitutions, and its contribution to the magnetic orbitals is roughly proportional to the energy splitting. The different behavior for the two classes of compounds upon addition of the pendant phenyl substituent can find a rationale when considering the changes of the molecular equilibrium geometry of D_1 induced by such substitution. In Figure 5, a side view of the optimized structures of diradicals Dp_1 and Dp_2 is reported, in the a and b panels, respectively. As far as the latter diradical is concerned, all the rings of the polycyclic moiety are coplanar, whereas in the diarylnitroxide diradical Dp_1, the angles between the lateral rings and central ring α_1 and α_2 (green arrows) are 117.5° and 116°, respectively. Furthermore, the torsional angle between the central ring and the pendant phenyl group is also different between the two compounds, increasing from 102° (ϕ_A, left

dx.doi.org/10.1021/ct300790c | J. Chem. Theory Comput. 2013, 9, 300−307

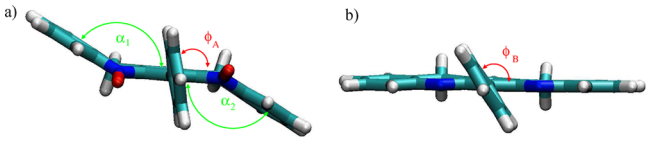

Figure 5. Side-views of the optimized structures of diradicals $\mathbf{Dp}_1$ (left) and $\mathbf{Dp}_2$ (right).

panel) to 125° (ϕ_B, right panel). In conclusion, it appears that the steric repulsion between the two oxygen atoms and the phenyl ring heavily distorts the polycyclic structure out of $\mathbf{Dp}_1$ planarity, thus affecting its capability to act as an efficient magnetic bridge, remarkably decreasing the singlet−triplet energy gap.

3.2. Aza-*m*-xylylene Diradical. The aza-*m*-xylylene derivative $\mathbf{A}_1$ (panel c of Figure 2) was recently reported[24] as the first example of ferromagnetic organic diradical persistent at room temperature in solution on the time scale of minutes. The ΔE_{ST} energy gap was estimated on the order of 10 kcal/mol. Besides confirming the agreement with the experimental estimates, calculations were performed to (i) evaluate the influence of the lateral chain lengths on the magnetic splitting; (ii) verify whether the conclusions drawn for the species discussed in the previous section can be extended to these new systems; (iii) investigate the effect of different structures embedding the *m*-phenylene "magnetic unit." To better address these issues, and to verify the possibility of adopting computationally convenient models, a slightly smaller model $\mathbf{A}_2$ of diradical $\mathbf{A}_1$ was devised by substituting the *iso*-propyl lateral chains with methyl groups, whereas an azoxy homologue $\mathbf{A}_3$ was designed from $\mathbf{A}_2$ by including two NO· groups in place of the N· ones. All structures are reported in Figure 6. Finally, as in the previous section, two different fragmentation schemes, shown in Figure 7, were employed for each target molecule.

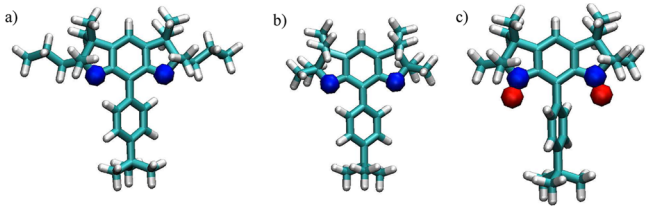

Figure 6. Target aza-*m*-xylylene and azoxy-*m*-xylylene diradicals: (a) aza-*m*-xylylene diradical $\mathbf{A}_1$, (b) model aza-*m*-xylylene diradical $\mathbf{A}_2$, (c) model azoxy-*m*-xylylene diradical $\mathbf{A}_3$. Atoms bearing the magnetic orbitals are evidenced with blue (N) and red (O) spheres.

In view of the previous results, DDCI calculations were performed within the three-step protocol considering a maximum VAVO/VO ratio of 60% for diradicals $\mathbf{A}_1$ and $\mathbf{A}_2$, and 40% for $\mathbf{A}_3$. Results for all homologues, summarized in Table 5, appear to validate this choice, since for the former diradicals A_1 and A_2, the variation of the ΔE_{ST} by increasing the VAVO/VO ratio from 40% to 60% is negligible (less than 0.1 kcal/mol)

The two different fragmentation schemes adopted for $\mathbf{A}_1$ result in a gap ΔE_{ST} of 11.7 and 10.0 kcal/mol, respectively. Similarly to the aminyl case ($\mathbf{D}_2$ and $\mathbf{Dp}_2$), it appears that the lateral five-membered rings should also be included in the primary fragment, as they account for ∼2 kcal/mol. When this is done, the obtained gap is again in very good agreement with the experimental value of 10 kcal/mol. The energy gap

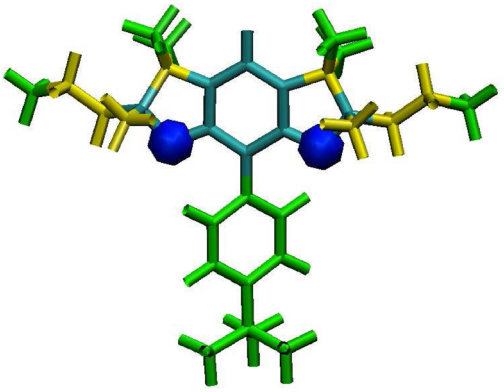

Figure 7. Fragmentation routes applied to diradical $\mathbf{A}_1$. Cyan: active fragment. Yellow: supplementary active fragment (route **2**). Green: external fragments. Atoms bearing the magnetic orbitals are always active and evidenced with blue (N) spheres. The same schemes have been used for homologues $\mathbf{A}_2$ and $\mathbf{A}_3$.

Table 5. DDCI Results for Target Diradicals $\mathbf{A}_1$, $\mathbf{A}_2$, and $\mathbf{A}_3$[a]

$\mathbf{A}_1$				
fragm. route	VAVO/VO (%)	ΔE_{ST}^{V} (cm^{-1})	ΔE_{ST} (cm^{-1})	ΔE_{ST} (kcal/mol)
1	40	4331	4074	11.7
1	50	4243	4079	11.7
1	60	4182	4089	11.7
2	40	3671	3490	10.0
2	50	3620	3505	10.0
2	60	3552	3520	10.0
$\mathbf{A}_2$				
fragm. route	VAVO/VO (%)	ΔE_{ST}^{V} (cm^{-1})	ΔE_{ST} (cm^{-1})	ΔE_{ST} (kcal/mol)
1	40	4277	4125	11.8
1	50	4250	4127	11.8
1	60	4196	4132	11.8
2	40	3481	3312	9.5
2	50	3441	3324	9.5
2	60	3361	3342	9.6
$\mathbf{A}_3$				
fragm. route	VAVO/VO (%)	ΔE_{ST}^{V} (cm^{-1})	ΔE_{ST} (cm^{-1})	ΔE_{ST} (kcal/mol)
2	40	472	284	0.8
2*	40	412	381	1.1

[a]Fragmentation route and VAVO/VO ratio are reported in the first two columns. In the third column, the magnetic splitting (ΔE_{ST}^{V}) obtained by a pure variational calculation is reported. In the last two columns, the CSPA corrected value is reported in cm^{-1} and kcal/mol, respectively. A asterisk designates values obtained for the same geometry of $\mathbf{A}_2$ without re-optimizing the molecular structure.

obtained for the model system $\mathbf{A}_2$ does not differ sensibly from those of the complete molecule $\mathbf{A}_1$ (≃12 and ≃10 kcal/mol computed in routes **1** and **2**, respectively). From a computational point of view, this is an important validation, as it allows one to substitute long aliphatic chains with shorter ones without sensibly affecting the magnetic properties of the system under study, but with obvious benefits in terms of time and feasibility. The massive effect coming with the substitution of the N· group with the NO· one is confirmed also on these diradicals. Indeed, the comparison of the results obtained for $\mathbf{A}_2$ and $\mathbf{A}_3$ systems shows again a reduction of the ΔE_{ST} gap by 1

order of magnitude. With the aim of separating the pure effect of the oxygen presence from the one due to geometrical rearrangement that we have underlined for the $\mathbf{Dp}_1$ species (Figure 5), two different geometries were taken into account for diradical $\mathbf{A}_3$. Besides the first structure, obtained with a complete geometry optimization as done for the previous systems, a second structure was devised (marked by an $*$ in Table 5) by simply attaching oxygen atoms to the nitrogen based radical $\mathbf{A}_2$, without any geometry reoptimization but the oxygen atoms themselves. As can be seen by comparing the last two rows of Table 5, the geometrical distortions further decrease the gap to less than 1 kcal/mol (roughly a 25% decrease).

In conclusion, **A** compounds are seen to yield larger gaps with respect to their **D** homologues for reasons related to the larger delocalization occurring in the latter compounds. In particular, two effects contribute to favoring the singlet state, hence decreasing the energy gap. First, the lateral aromatic rings, present in **D** compounds, draw some electron charge density away from the central ring, with the consequence of making it a less effective ferromagnetic molecular bridge. Second, owing to the higher delocalization induced in the magnetic orbitals, the lateral aromatic rings favor the charge transfer configurations which only contribute to stabilizing the singlet state.

A final issue that might be worth addressing is the effect of the employed geometry on the computed singlet−triplet gap. For the $\mathbf{A}_2$ diradical, a new geometry was obtained by performing a QM optimization at the PBE0/cc-pvDZ level, obtaining $\Delta E_{ST} \sim 9.8$ kcal/mol, in good agreement with the 9.5 kcal/mol of Table 5. Considering that the two computed geometries differ at most by ∼0.01 Å on bond lengths and 1° and 2° on angles and dihedrals, respectively, this agreement is not surprising. As far as the **D** species are concerned, a different strategy was followed. Indeed, a new geometry of the $\mathbf{Dp}_2$ diradical was obtained from the X-ray crystallographic file of the parent diamine molecule[40] by proper substitution/deletion of non-matching atoms. This geometry sensibly differs from the B3LYP one. Besides the sensible distortion (∼76°) of almost 20° found for dihedral ϕ_B (see Figure 5), the differences between the two $\mathbf{Dp}_2$ geometries are about three times those found in the former $\mathbf{A}_2$ case. This in turn reflects a larger discrepancy on the computed ΔE_{ST} value, 3.82 kcal/mol being found for the reconstructed geometry vs the 5.52 kcal/mol of Table 3. This last finding suggests that geometries reconstructed from experimental data obtained for parent species should be used with some care, and QM optimized geometries should be preferred when direct experimental information is missing.

4. CONCLUSIONS

The accurate yet feasible multireference method for the calculation of isotropic magnetic splitting, implemented and validated in our group,[34,61,63] has been here applied to several promising organic diradicals, recently reported in the literature[24,32,33] as possibly relevant in the field of spintronics. The capability of accurately evaluating the singlet triplet energy gap is particularly important in these prototypes of organic magnets, since only a lower limit of ΔE_{ST} can be estimated experimentally.[32] Reliable calculations also allow for a rationalization of the effects that different chemical environments may have on the singlet−triplet energy gap. Moreover, accurate theoretical studies can aid the design of such new materials, with obvious advantages in terms of cost and time.

For all of the investigated compounds, the computed ΔE_{ST}'s agree well with the lower bounds estimated by the experiment. On the contrary, as already noted in the literature,[33,44,45] it seems to be confirmed that the lower level BS-DFT approach overestimates the gap quite significantly, providing magnetic splittings of 2,[32] 7,[33] and 11 kcal/mol[24] for diarylnitroxide, aminyl, and aza-*m*-xylylene diradicals, respectively, to be compared with 0.5, 4.7, and 9.5 kcal/mol as calculated at the post-HF DDCI level in this paper. The striking drop in the magnetic splitting, registered when the NO· group is present instead of N·, is also well reproduced and interpreted in terms of both spin delocalization and geometrical distortion. By extending the calculations to several other homologues, it appears that this is a general issue, since the presence of the NO· group strongly reduces the efficiency of the *meta* substituted phenyl as a ferromagnetic bridge. The presence of substituted pendant phenyls on the bridge, which through their steric encumbrance[24] favor the chemical stability of the diradical species, shows modest effects on the magnetic properties. The indication that can be drawn from the comparison of more promising radicals, i.e., aminyl and aza-*m*-xylylene molecules, is that reducing the extent of the (partially) conjugated structure embedding the "magnetic" *m*-phenylene unit, the ferromagnetic coupling induced by the central *meta* substituted phenyl is enhanced.

In conclusion, the proposed three step multireference post-HF calculations can be applied to the computation of the singlet triplet energy gap of rather large organic diradicals. Furthermore, the soundness of the theory underlying CI methods allows for a reliable rationalization of the relationships between the molecular structure and the chemical details of the investigated diradicals. In turn, this rationalization may flank the experiment and aid both the synthesis and the characterization of novel organic magnets. From a theoretical viewpoint, the experience gained in the present work furnishes sound criteria for the choice of fragmentation scheme based on population analysis of the magnetic orbitals.

AUTHOR INFORMATION

Corresponding Author

*E-mail: giacomo.prampolini@pi.ipcf.cnr.it.

Notes

The authors declare no competing financial interest.

REFERENCES

(1) Rajca, A. *Chem. Rev.* **1994**, *94*, 871−893.
(2) Rajca, A.; Wongsriratanakul, J.; Rajca, S. *Science* **2001**, *294*, 1503−1505.
(3) Kahn, O. *Molecular Magnetism*; VCH Publishers, Inc.: New York, 1993.
(4) Coronado, E.; Delhaès, P.; Gatteschi, D.; Milles, J. S. *Molecular Magnetism: From Molecular Assemblies to the DeVice*; Kluwer Academic Publishers: Dordrecht, 1995; NATO ASI Series E, Vol. *321*.
(5) Gatteschi, D.; Sessoli, R.; Villain, J. *Molecular Nanomagnets*; Oxford University Press: Oxford, U. K., 2006; Vol. *5* of Mesoscopic Physics and Nanotechnology.
(6) Rajca, A.; Wongsriratanakul, J.; Rajca, S. *J. Am. Chem. Soc.* **2004**, *126*, 6608−6626.
(7) Fukuzaki, E.; Nishide, H. *J. Am. Chem. Soc.* **2006**, *128*, 996−1001.
(8) Rajca, A.; Boratynski, P. J.; Olankitwanit, A.; Shiraishi, K.; Pink, M.; Rajca, S. *J. Org. Chem.* **2012**, *77*, 2107−2120.
(9) Zhdanov, R. *Bioactive Spin Labels*; Springer-Verlag: Berlin, 1992.

(10) Marx, L.; Rassat, A. *Chem. Commun.* **2002**, 632−633.
(11) Francese, G.; Dunand, F.; Loosli, C.; Merbach, A.; Decurtins, S. *Magn. Reson. Chem.* **2003**, *41*, 81−83.
(12) Spagnol, G.; Shiraishi, K.; Rajca, S.; Rajca, A. *Chem. Commun.* **2005**, 5047−5049.
(13) Matsuda, K.; Iwamura, H. *Curr. Opin. Solid State Mater. Sci.* **1997**, *2* (4), 446−450.
(14) Koivisto, B. D.; Hicks, R. G. *Coord. Chem. Rev.* **2005**, *249*, 2612−2630.
(15) Murata, H.; Miyajima, D.; Nishide, H. *Macromolecules* **2006**, *39*, 6331−6335.
(16) Itoh, T.; Hirai, K.; Tornioka, H. *Bull. Chem. Soc. Jpn.* **2007**, *80*, 138−157.
(17) Nishimaki, H.; Ishida, T. *J. Am. Chem. Soc.* **2006**, *132*, 9598−9599.
(18) Lee, J.; Lee, E.; Kim, S.; Bang, G. S.; Shultz, D. A.; Schmidt, R. D.; Forbes, M. E.; Lee, H. *Angew. Chem., Int. Ed.* **2011**, *50*, 4415.
(19) Steinberg, B.; Jackson, E.; Filatov, A.; Wakamiya, A.; Petrukhina, M.; Scott, M. *J. Am. Chem. Soc.* **2009**, *131*, 10537−10545.
(20) Valenti, G.; Bruno, C.; Rapino, S.; Marcaccio, M.; Paolucci, F.; Jackson, E.; Scott, L. *J. Phys. Chem. C* **2010**, *114*, 19467−19472.
(21) Fort, E.; Scott, L. *Angew. Chem., Int. Ed.* **2010**, *49*, 6626−6628.
(22) Ratera, I.; Veciana, J. *Chem. Soc. Rev.* **2012**, *41*, 303−349.
(23) Lahti, P. *Adv. Phys. Org. Chem.* **2011**, *45*, 93−169.
(24) Olankitwanit, A. R. A.; Rajca, S. *J. Am. Chem. Soc.* **2011**, *133*, 4750−4753.
(25) Yu, L.; Chen, M.; Dalton, L. *Chem. Mater.* **1990**, *2*, 649−659.
(26) Kim, F.; Ren, G.; Jenekhe, S. *Chem. Mater.* **2011**, *23*, 682−732.
(27) Facchetti, A. *Chem. Mater.* **2011**, *23*, 733−758.
(28) Dong, A.; Wang, C.; Hu, W. *Chem. Commun.* **2010**, *46*, 5211−5222.
(29) Rajca, A.; Rajca, S.; Padmakumar, R. *Angew. Chem., Int. Ed.* **1994**, *33*, 2091−2093.
(30) Rajca, A.; Lu, K.; Rajca, S. *J. Am. Chem. Soc.* **1997**, *119*, 10335−10345.
(31) Rajca, A.; Wongsriratanakul, J.; Rajca, S.; Cerny, R. *Chem.—Eur. J.* **2004**, *10*, 3144−3157.
(32) Rajca, A.; Shiraishi, K.; Rajca, S. *Chem. Commun.* **2009**, 4372−4374.
(33) Boratynski, P. J; Pink, M.; Shiraishi, K.; Rajca, S.; Rajca, A. *Angew. Chem., Int. Ed.* **2010**, *49*, 5459−5462.
(34) Barone, V.; Cacelli, I.; Ferretti, A.; Monti, S.; Prampolini, G. *J. Chem. Theory Comput.* **2011**, *7*, 699−706.
(35) Ishida, T.; Iwamura, H. *J. Am. Chem. Soc.* **1991**, *113*, 4238−4241.
(36) Kurokawa, G.; Ishida, T.; Nogami, T. *Chem. Phys. Lett.* **2004**, *392*, 74−79.
(37) Nishimaki, H.; Mashiyama, S.; Yasui, M.; Nogami, T.; Ishida, T. *Chem. Mater.* **2006**, *18*, 3602−3604.
(38) Rajca, A.; Lu, K.; Rajca, S.; Ross, C., II. *Chem. Commun.* **1999**, 1249−1250.
(39) Rajca, A.; Vale, M.; Rajca, S. *J. Am. Chem. Soc.* **2008**, *130*, 9099−9105.
(40) Rajca, A.; Shiramishi, K.; Pink, M.; Rajca, S. *J. Am. Chem. Soc.* **2007**, *129*, 7232−7233.
(41) Dvolaitzky, M.; Chiarelli, R.; Rassat, A. *Angew. Chem., Int. Ed.* **1992**, *31*, 180−181.
(42) Noodleman, L.; Norman, J. G. *J. Chem. Phys.* **1979**, *70*, 4903−4906.
(43) Noodleman, L. *J. Chem. Phys.* **1981**, *74*, 5737−5713.
(44) Quast, H.; Ndling, W.; Klemm, G.; Kirshfield, A.; Neuhaus, P.; Sander, W.; Hrovat, D.; Borden, W. T. *J. Org. Chem.* **2008**, *73*, 4956−4961.
(45) Amiri, S.; Schereiner, P. *J. Phys. Chem. A* **2009**, *113*, 11750−11757.
(46) Queralt, N.; Taratiel, D.; de Graaf, C.; Caballol, R.; Cimiraglia, R.; Angeli, C. *J. Comput. Chem.* **2008**, *29*, 994−1003.
(47) de Loth, P.; Cassoux, P.; Daudey, J. P.; Malrieu, J. P. *J. Am. Chem. Soc.* **1981**, *103*, 4007−4016.
(48) Miralles, J.; Daudey, J.; Caballol, R. *Chem. Phys. Lett.* **1992**, *198*, 555−562.
(49) Castell, O.; Caballol, R.; Subra, R.; Grand, A. *J. Phys. Chem.* **1995**, *99*, 154.
(50) de Graaf, C.; Sousa, C.; de, I.; Moreira, P. R.; Illas, F. *J. Phys. Chem. A* **2001**, *105*, 11371−11378.
(51) Angeli, C.; Calzado, C. J.; Cimiraglia, R.; Evangelisti, S.; Guihéry, N.; Leininger, T.; Malrieu, J.-P.; Maynau, D.; Ruitz, J. V. P.; Sparta, M. *Mol. Phys.* **2003**, *101*, 1389.
(52) Neese, F. *J. Chem. Phys.* **2003**, *119*, 9428.
(53) Calzado, C. J.; Cabrero, J.; Malrieu, J. P.; Caballol, R. *J. Chem. Phys.* **2002**, *116*, 3985−4000.
(54) de Graaf, C.; Caballol, R.; Romo, S.; Poblet, J. M. *Theor. Chem. Acc.* **2009**, *123*, 3.
(55) Calzado, C. J.; Angeli, C.; Caballol, R.; Malrieu, J.-P. *Theor. Chem. Acc.* **2010**, *126*, 185.
(56) Calzado, C. J.; Angeli, C.; de Graaf, C.; Caballol, R. *Theor. Chem. Acc.* **2011**, *128*, 505.
(57) Miralles, J.; Castell, O.; Caballol, R.; Malrieu, J. *Chem. Phys.* **1993**, *172*, 33−43.
(58) Calzado, C. J.; Cabrero, J.; Malrieu, J. P.; Caballol, R. *J. Chem. Phys.* **2002**, *116*, 2728−2747.
(59) Barone, V.; Cacelli, I.; Ferretti, A. *J. Chem. Phys.* **2009**, *130*, 094306.
(60) Barone, V.; Cacelli, I.; Ferretti, A.; Prampolini, G. *Phys. Chem. Chem. Phys.* **2009**, *11*, 3854−3860.
(61) Barone, V.; Cacelli, I.; Ferretti, A.; Prampolini, G. *J. Chem. Phys.* **2009**, *131*, 224103.
(62) Barone, V.; Cacelli, I.; Cimino, P.; Ferretti, A.; Monti, S.; Prampolini, G. *J. Phys. Chem. A* **2009**, *113*, 15150−15155.
(63) Barone, V.; Cacelli, I.; Ferretti, A.; Monti, S.; Prampolini, G. *Phys. Chem. Chem. Phys.* **2011**, *13*, 4709−4714.
(64) Frisch, M. J.; Trucks, G. W.; Schlegel, H. B.; Scuseria, G. E.; Robb, M. A.; Cheeseman, J. R.; Scalmani, G.; Barone, V.; Mennucci, B.; Petersson, G.; Nakatsuji, H.; Caricato, M.; Li, X.; Hratchian, H. P.; Izmaylov, A. F.; Bloino, J.; Zheng, G.; Sonnenberg, J. L.; Hada, M.; Ehara, M.; Toyota, K.; Fukuda, R.; Hasegawa, J.; Ishida, M.; Nakajima, T.; Honda, Y.; Kitao, O.; Nakai, H.; Vreven, T.; Montgomery, J. A.; Peralta, J. E.; Ogliaro, F.; Bearpark, M.; Heyd, J. J.; Brothers, E.; Kudin, K. N.; Staroverov, V. N.; Kobayashi, R.; Normand, J.; Raghavachari, K.; Rendell, A.; Burant, J.; Iyengar, S. S.; Tomasi, J.; Cossi, M.; Rega, N.; Millam, J. M.; Klene, M.; Knox, J. E.; Cross, J. B.; Bakken, V.; Adamo, C.; Jaramillo, J.; Gomperts, R.; Stratmann, R. E.; Yazyev, O.; Austin, A. J.; Cammi, R.; Pomelli, C.; Ochterski, J. W.; Martin, R. L.; Morokuma, K.; Zakrzewski, V. G.; Voth, G. A.; Salvador, P.; Dannenberg, J. J.; Dapprich, S.; Parandekar, P. V.; Mayhall, N. J.; Daniels, A. D.; Farkas, O.; Foresman, J. B.; Ortiz, J. V.; Cioslowski, J.; Fo, D. J. *Gaussian 09*, revision c.01; Gaussian, Inc.: Wallingford CT, 2009.
(65) Schmidt, M. W.; Baldridge, K. K.; Boats, J. A.; Elbert, S. T.; Gordon, M. S.; Jensen, J. H.; Koseki, S.; Matsunaga, N.; Nguyen, K. A.; Su, S. J.; Windus, T. L.; Dupuis, M.; Montgomery, J. A. *J. Comput. Chem.* **1993**, *14*, 1347−1363.
(66) Pipek, J.; Mezey, P. G. *J. Chem. Phys.* **1989**, *90*, 4916−4926.
(67) Barone, V.; Cacelli, I.; Ferretti, A.; Girlanda, M. *J. Chem. Phys.* **2008**, *128*, 174303.
(68) Angeli, C.; Calzado, C. J. *J. Chem. Phys.* **2012**, *137*, 034014.